Transverse 2-D Gliding Arc Modeling

Alexander F. Gutsol and Shailesh P. Gangoli

Abstract— **This paper was prepared in response to the growing interest in the numerical simulation of the gliding arc (GA) discharge. Our approach is rather simple 2-D modeling of the GA, in the plane that is parallel to the gas flow and perpendicular to the discharge current. We used Fluent software with a subroutine that calculates electric conductivity of argon plasma and local heat release due to the electric current of predetermined value. Electric conductivity of argon was calculated as function of the reduced electric field and gas temperature. Our results show that this approach can give very useful information about the gas-discharge interaction, which is very important to capture the discharge behavior. Presence of discharge inside the gas flow significantly disturbs both of them. Gas-discharge slip velocity exists at least at the beginning of GA development cycle even if there is no mechanism of the discharge deceleration. Just original spark formation associated with the electrode surfaces results in the appearance of this "independent" slip. In the cases of reasonably high gas velocities and discharge currents, this initial slip does not disappear during the discharge lifetime and can result in significant discharge cross-sectional elongation along the gas flow. Electric field fluctuation at any particular part of the discharge channel can be very large, and this can have the major effect on the nonequilibrium ionization and chemical processes.**

Index Terms— **Argon plasma electric conductivity, atmospheric-pressure plasma devices, computational fluid dynamics (CFD) modeling, discharge–flow interaction, gliding arc (GA), plasma simulations.**

I. Introduction

THE gliding arc (GA) discharge introduced by Czernichowski [1], still attracts many researchers. It became especially popular after the introduction of newer designs, such as the magnetic GA (plasma disc) and GA in Tornado (GAT) [2]. In just one journal, the IEEE TRANSACTIONS ON PLASMA SCIENCE, since 2014, nine different research groups have published papers related to GAs [3]–[11]. GA is attractive because of its relative technical simplicity and intermediate "warm plasma" properties. On the other hand, because of its non-stationary and 3-D nature, it is rather difficult to numerically model the GA.

Preliminary results of this paper were obtained in 2006 at the Drexel Plasma Institute and presented at the Gordon Conference on Plasma Processing Science but were not submitted for publication till now. The motivation to rekindle and present this paper came from our belief that these results can provide crucial guidance to other researchers looking to model the GA discharge.

Relatively recently, the PLASMANT Group from the University of Antwerp started a project on GA numerical modeling with the goal to make 3-D model of nonequilibrium discharge, including chemical reactions, e.g., CO_2 dissociation [12]–[14]. In general, the modeling of arcs in gas flow is not new, as it can be seen, for example, in publication [15]. More information can be found in recent publications [16], [17]. These papers show results of the 3-D gas-discharge interaction modeling, including magnetohydrodynamics. Therefore, a reasonable question arises–what is the problem in GA modeling? There are several fundamental problems: (1) Conventional approach in arc modeling assumes local thermodynamic equilibrium, and this approach cannot be applied for low-current gliding discharges. By the way, these discharges are sometimes GAs and other times they are gliding glow discharges [18]. However, the term GA is used rather broadly, and we will continue to use it in this paper. (2) Conventional high current arc has very high temperature and it is therefore not "transparent" to gas with only a negligible portion of the gas flow being able to penetrate into a discharge channel. (3) Gas viscosity in conventional high temperature arc plasma reactors is very high, and gas flow assumed to be laminar. This is usually not the case for GA reactors.

The PLASMANT Group started with rather detailed nonequilibrium model of Ar plasma and two 2-D models of the discharge channel: an axisymmetric one without gas motion, and a Cartesian one, where an infinite plasma "sheet" is bending and elongating by gas flow, and is artificially decelerated at electrode spots [12]. Yes, the results obtained using the second approach looks like GA, and this is good already, however, is the model able to capture major GA peculiarities? Why should we believe that the channel is axisymmetric at least locally? What controls the electrode spot motion and gas-discharge slip velocity? And how the slip velocity can be seen and calculated in these models? Later, when this paper was already submitted as an abstract for ICOPS, the PLAMANT Group published another paper [14] with 3-D modeling of small GAT reactor, where some slip velocity should be observed, but the authors did not emphasize this, probably because their approach of separation of gas-dynamics and discharge modeling limits the ability to reveal this important feature. According to the paper [14], "In order to reduce the computation time, the gas flow model was solved first as a stationary problem and the obtained velocity field and the turbulent energy dissipation were used in the plasma model coupled with the gas heating. Thus, the model does not consider the hydrodynamic influence of the GA on the gas flow."

Manuscript received August 31, 2016; revised October 30, 2016; accepted November 20, 2016. Date of publication January 31, 2017; date of current version April 10, 2017.

A. F. Gutsol is with Chevron Energy Technology Company, Richmond, CA 94801 USA (e-mail: gutsol@chevron.com).

S. P. Gangoli is with Air Products and Chemicals, Inc., Allentown, PA 18105 USA (e-mail: gangolsp@airproducts.com).

Color versions of one or more of the figures in this paper are available online at http://ieeexplore.ieee.org.

Digital Object Identifier 10.1109/TPS.2017.2653841

On the other hand, our model is probably oversimplified from the standpoint of plasma description, although it includes thermal and non-thermal ionization and recombination reactions. Our model couples nonstationary gas-dynamics with gas heating by electric current, and this coupling helps reveal (at least qualitatively) the interaction between discharge and gas flow. We hope that the information that was obtained using our simple approach will help other researchers, e.g., the PLASMANT Group, in their efforts to make meaningful 3-D model of GA using limited computational resources.

II. Model Description

Like the PLASMANT Group, we also modeled the gliding discharge in argon. As our goal was to qualitatively study the interaction between discharge and gas flow, we have used rather simple approach for modeling of Ar plasma properties (Fig. 1) and used these properties with Fluent computational fluid dynamics (CFD) software. In low current discharges without external magnetic fields, electromagnetic forces are small, and discharge influence on gas dynamics is expressed by the spatial heating effect. Therefore, the major parameters we need for simulation of the discharge–flow interaction in CFD are electric conductivity and Joule heating. We assumed that argon plasma electric conductivity σ_{tot} can be presented as a sum of the nonequilibrium electric conductivity σ_{ne} and the electric conductivity determined by the thermal processes σ_{temp}: $\sigma_{\text{tot}} = \sigma_{\text{ne}} + \sigma_{\text{temp}}$. For calculation of the nonequilibrium electric conductivity, we need electron mobility μ_e and electron number density N_e: $\sigma_{\text{ne}} = e \cdot \mu_e \cdot N_e$, where e is the electron charge. For calculation of electron mobility, we used Bolsig+ simulation considering only the most important interactions of electrons with argon atoms: elastic collisions, excitation to the 11.5 eV level and ionization (ionization potential $E_i = 15.8$ eV). Electron number density N_e was calculated from the balance between ionization rate from the ground state and the recombination. Ionization coefficient was calculated within the Bolsig+ simulation. Ten years after the start of this paper, we are unable to find the information source for the recombination rate that we selected, however the resultant N_e dependence on the reduced electric field E/N_0 (Fig. 2) looks reasonable, and corresponds approximately to two possible cases (a) three-body recombination with the recombination rate coefficient $k_R \sim 10^{-32}\text{m}^6/\text{s}$, or (b) dissociative attachment to Ar_2^+ ions, that looks probably more realistic (see [19]), with the recombination rate $k_A = 8.8 \cdot 10^{-14} \cdot T_e^{-0.67}$ m^3/s taken from [20]. In the first case the balance looks like

$$k_I N_e N_0 = k_R N_e^3 \tag{1}$$

while, in the second case the balance looks like

$$k_I N_e N_0 = k_A N_e^2 \tag{2}$$

because concentration of Ar_2^+ ions is almost equal N_e [19].

Numerically, the curve in Fig. 2 was represented by three parts:

1) For $E/N_0 < 6$, $N_e = 0$.
2) For $6 \le E/N_0 < 8$, $N_e = 10^{(4.692(E/N-6)+6)}$ (m^{-3}).

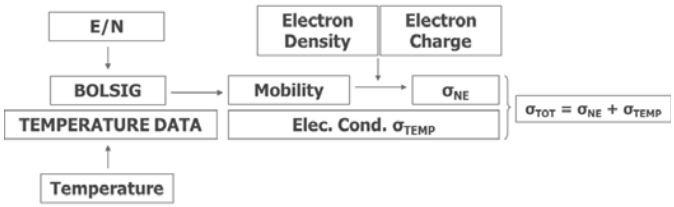

Fig. 1. Schematic for calculation of plasma conductivity.

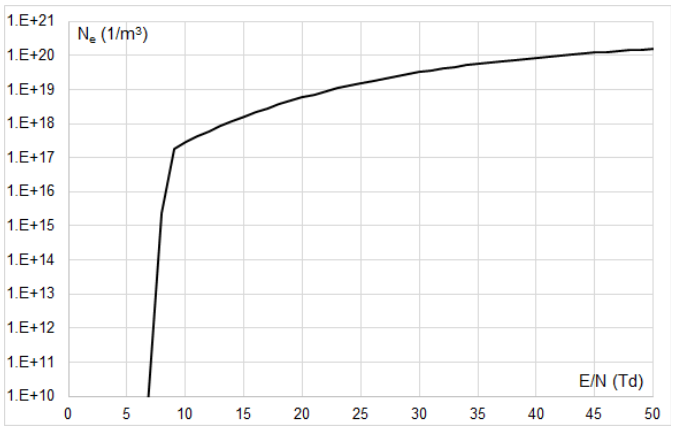

Fig. 2. Dependence of electron number density N_e on the reduced electric field E/N_0 used for calculation of nonequilibrium electric conductivity σ_{ne}.

3) For $8 \le E/N_0$
$N_e = 10^{(14.24\exp(0.0002942E/N)-5.16\exp(-0.05986E/N)+6)}$ (m^{-3}).

Electric conductivity of argon plasma at high temperatures ($T_0 > 5370$ K) was measured and evaluated by many authors, and these data were collected in the book by Dresvin [21, p. 141]. This high-temperature portion of σ_{temp} was approximated by the formula $\sigma_{\text{temp}} = -3.464 \cdot 10^{-9} T_0^3 + 1.235 \cdot 10^{-4} T_0^2 - 0.4969 T_0 - 356.2 (\text{Ohm}^{-1}\text{m}^{-1})$. At lower temperatures, equilibrium electric conductivity was estimated using the Saha equation ([22, p. 281] or [23, p. 196]) as

$$\sigma_{\text{temp}}(T) = C \cdot \exp(-E_i/(2k_B T_0)) \tag{3}$$

where $k_B = 8.617 \cdot 10^{-5}$ eV/K is the Boltzmann's constant, and the constant $C = 1.0038 \cdot 10^7$ $\text{Ohm}^{-1}\text{m}^{-1}$ was selected to give the same σ_{temp} value at $T_0 = 5370$ K as the high temperature dependence (see above). The whole equilibrium electric conductivity dependence on temperature used in simulation is shown in Fig. 3.

Calculation of plasma conductivity was included into the specially written subroutine file for Fluent. The major role of this subroutine (Fig. 4) was iterative calculation of the Joule heating power in each cell of the simulation domain. To calculate Joule heating, in addition to conductivity we need an electric field value. Initially, rather low electric field $E = 100$ V/m, constant for the whole domain, was taken. Then, the total current value I_t calculated in the iteration cycle was compared with the predetermined (total required) current value I_{tr}. This comparison resulted in the adjustment of the electric field value, and a new iteration cycle started. To make the calculation procedure stable, we used an under-relaxation factor k of appropriate value $k \ll 1$.

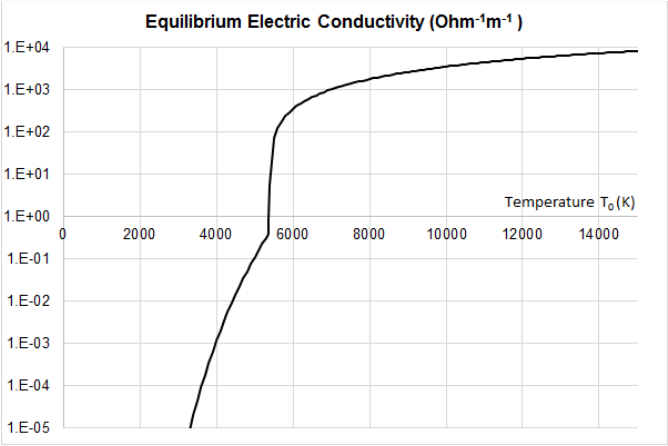

Fig. 3. Dependence of equilibrium electric conductivity σ_{temp} of argon plasma on temperature T_0 used in simulation.

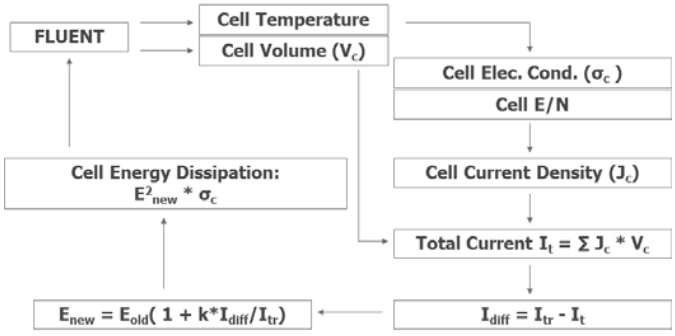

Fig. 4. Schematic of interaction of Fluent with a subroutine for the Joule power calculation in each cell of the simulation domain.

The total required current was kept constant, because it is rather stable parameter during GA evolution. In the case of the simplest system with constant voltage power supply and ballast resistor, usually current value reduces two times from the ignition moment to the extinction, in the absence of so-called "overshooting" effect [24]. Even more stable is current in advanced systems like magnetically stabilized GA [25], [26] or GAT flow [27], [28].

Now, when we discussed the power calculation procedure, it is worth coming back to the total electric conductivity discussion and show its dependence on both, temperature and electric field (not E/N_0) in the relevant range of parameters (Fig. 5).

As it will be seen later, in our simulation, the gas temperature T_0 never exceeds 5000 K, therefore the equilibrium part of the electric conductivity is presented by a smooth curve ($E = 0$). On the other hand, the nonequilibrium part is much larger at low temperatures, therefore the total electric conductivity σ_{tot} is presented by a group of "broken" curves in Fig. 5, resulting from the "broken" electron density curves in Fig. 2.

Joule heating power dependence on electric field (Fig. 6) is much stronger than that of electric conductivity, and as it will be seen from the simulation results, they are mostly depend on the nonequilibrium part of the electric conductivity.

All results presented in this paper were produced using the same rectangular domain of 15 cm height and 2 cm width

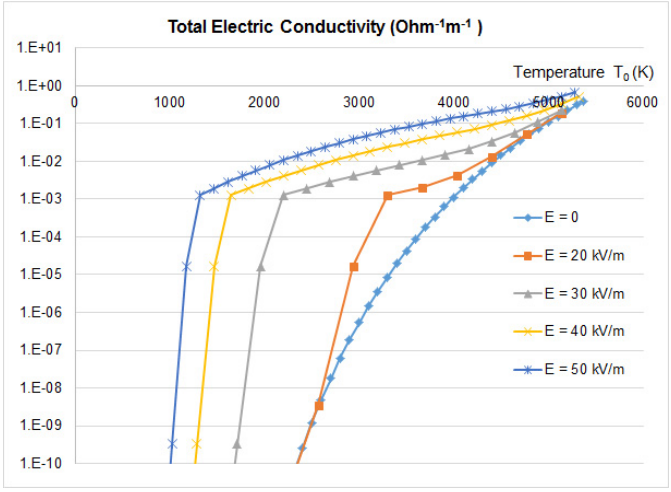

Fig. 5. Dependence of total electric conductivity σ_{tot} of argon plasma on temperature T_0 and electric field E.

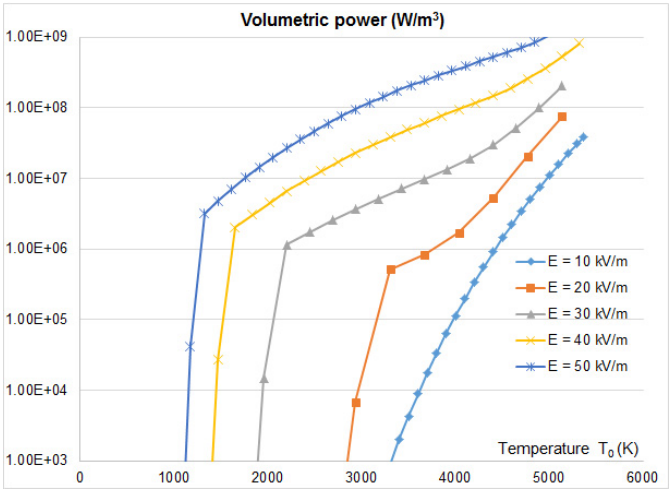

Fig. 6. Dependence of volumetric power release (W/m^3) in argon plasma on temperature T_0 and electric field E.

with the same unstructured mesh (Fig. 7) that was generated in 2006. This geometry approximately corresponds to the cross section of the plasma channel of the GA reactor (Fig. 8) made in 2000 at the University of Illinois at Chicago. Argon flow moves upwards, starting with uniform vertical velocity at the inlet (bottom of the domain). Method of plasma initiation was the following: In the beginning of CFD simulation, just after solution initialization, we patch gas with initial temperature of 700 K in a 5 mm circle near the inlet (see bottom right corner in Fig. 8). Then simulation starts and an initial electric field of 100 V/m is applied in the whole domain. Room temperature boundary conditions were applied to the gas flow at the inlet and to the side walls. Buoyancy force was not considered in the simulation.

It is necessary to explain, why we selected the plasma initiation procedure described above. Flow initialization by Fluent creates initial velocity distribution that is rather close to that of the cold flow in our very simple geometry. Patching a part of this flow with a high temperature at a particular spot in the domain imitates the formation of initial conductive

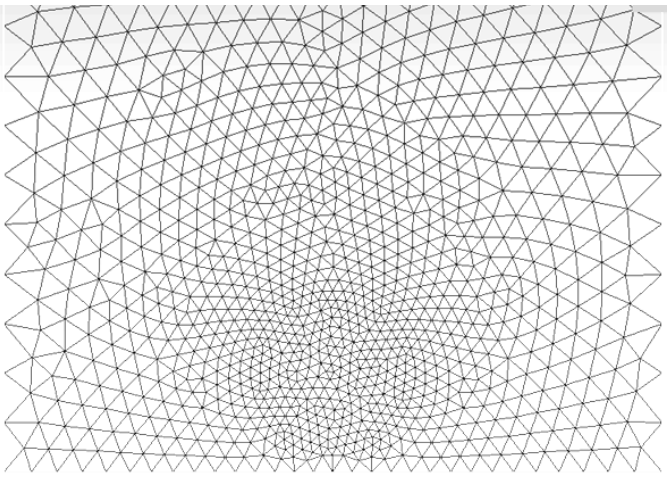

Fig. 7. Unstructured grid of the lower part (near the gas inlet) of the 15×2 cm simulation domain. Circular part of the grid was used for plasma initiation.

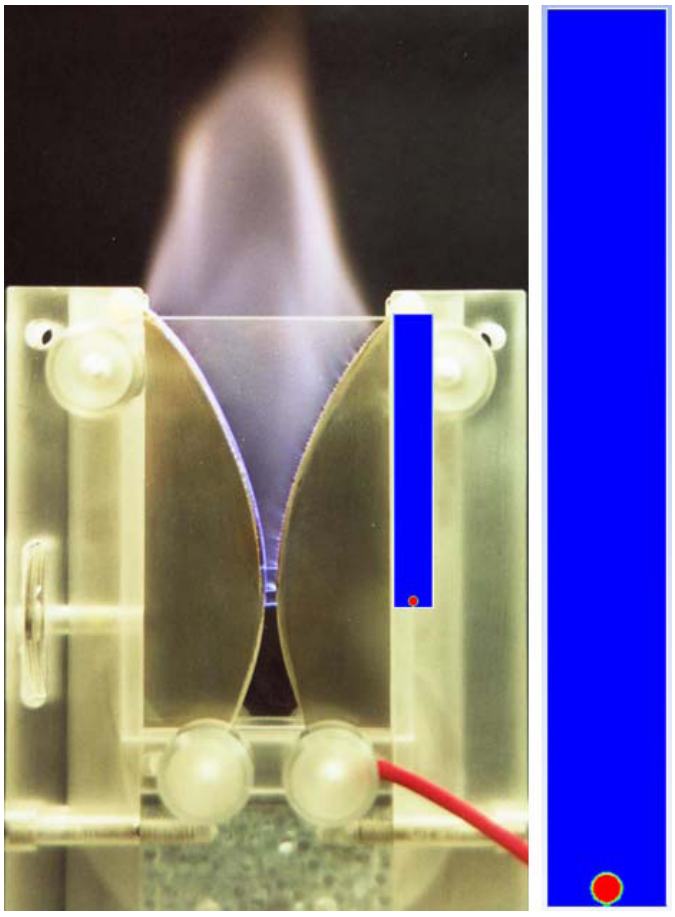

Fig. 8. Simulated GA reactor with superimposed simulation domain (GA reactor transverse cross section) after application of the high temperature patch procedure. Enlarged domain is shown to the right.

channel in the gas flow just after electric breakdown. On the one hand it forms inside the moving flow; on the other hand, during formation, it is attached to the stationary electrodes. In practice, during GA initiation, we hear sound from a spark, because it produces shock wave. Looking at the discharge initiation portion of the photo in Fig. 8, it is possible to estimate that the initial spark channel diameter is about 0.5 mm. As temperature in the channel is much larger than the room one, for rough estimation we can assume that all gas from the channel is pushed out radially and this creates a shock wave. The wave will propagate as a shock until its amplitude drops below about 50 Pa [29]. For simplification, we can assume that pressure inside the shock wave cylinder is constant in space (in reality, the wave amplitude is significantly larger than the average pressure behind it). In that case it is easy to estimate that the cylinder volume will be 2000 times larger than the volume of the spark, means that the shock wave will propagate at least to diameter of 2 cm. Very high speed of the shock wave itself and high radial speed of gas behind it wipes out the flow structure that existed before (in the case of Fig. 8 gas velocity was about 5 m/s), and only after relaxation of this radial flow, interaction of the discharge channel with the surrounding flow begins. Thus, as spark forms from the streamer channel that is attached to the electrodes, initial spark channel is stationary relative to the electrodes. Nevertheless, our approach consider the initial velocity to some extent. The readers should understand that this is very simplified approach because the breakdown stage is omitted completely. Rather large diameter and rather low temperature of the "high temperature" patch were selected to avoid instabilities at the initial simulation.

CFD simulation was made in transient regime, and this allowed us to create "movies" that demonstrate GA development in different regimes. In this paper, we present snapshots from these movies and variation in plasma properties during the cycle of GA development. In different simulation runs, we changed the total required current value I_{tr} and the initial gas flow velocity. Laminar or turbulent conditions were applied at different runs.

III. Simulation Results and Discussions

The lowest current simulated was 3 mA with initial gas speed of 1 m/s and laminar flow regime. Fig. 9 demonstrates gas temperature distribution at time step of 0.1 s. Fig. 10 presents evolution of GA maximal temperature and axial position of the maximal temperature spot on time.

Even this very low current and low velocity case with weak gas disturbance shows some interesting features. Look at the "three-angular" shape of the current channel. It is very different from the axisymmetric shape assumed in the paper [12]. During the initial development stage, current contraction and therefore temperature growth takes place. Probably, this is opposite to what happens in reality: small diameter spark transformation to a diffuse discharge. Temperature rise at the very end of the evolution cycle takes place because of the arc area reduction when it moves to the very end of the domain. There is an obvious "slip" between gas and discharge velocities in the beginning of a cycle. Thus, there is an "inertia" of the low-density plasma. This inertia is caused by the portions of gas decelerated during initial high-temperature channel formation. Note that at the end of the evolution, axial discharge velocity exceeds the initial gas velocity. This is caused by gas heating and therefore thermal expansion. As a

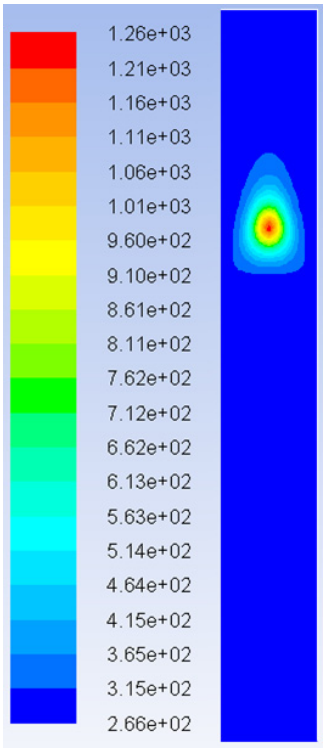

Fig. 9. Contours of gas temperature T_0(K) at time step of 0.1 s for 3 mA–1 m/s case.

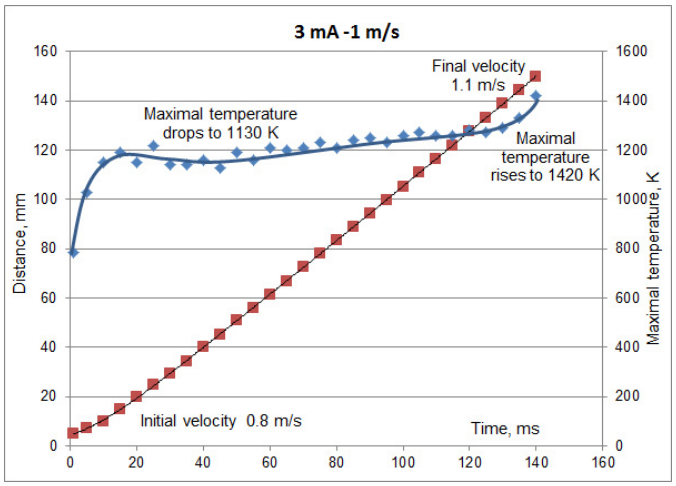

Fig. 10. Evolution of GA maximal temperature and axial position of the maximal temperature spot for 3 mA–1 m/s case.

result, gas above the discharge should move faster than below, and the discharge itself should move with an intermediate speed.

Some additional features were better revealed during simulation of the 35 mA–1 m/s case. Let's consider contours of stream function (Fig. 11), temperature and vertical velocity (Fig. 12) at the time step of 9 ms. Fig. 11 clearly demonstrates that gas expulsion from the discharge channel is not very significant (gas penetration into discharge channel is typical for nonthermal discharges with convective cooling) despite rather high maximal gas temperature (Fig. 12). Though the

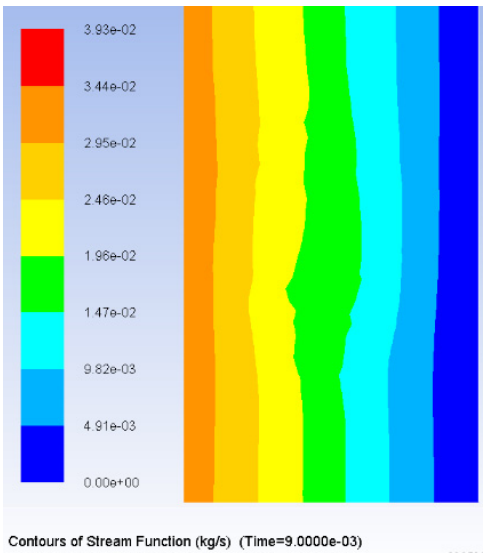

Fig. 11. Contours of stream function at time step of 9 ms for 35 mA–1 m/s case.

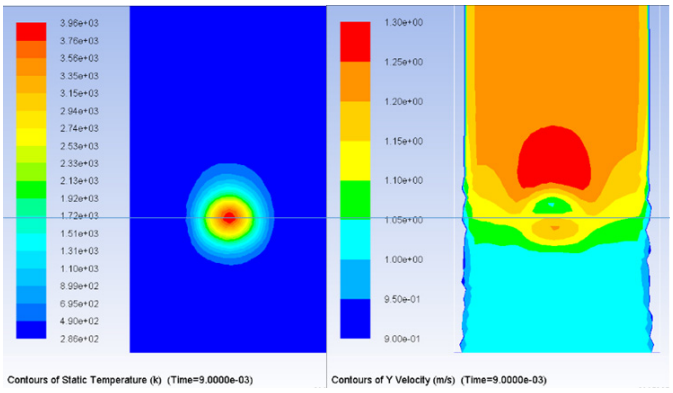

Fig. 12. Contours of gas temperature and axial gas velocity at time step of 9 ms for 35 mA–1 m/s case. Horizontal line shows the axial position of temperature maximum.

difference between the initial gas and the discharge channel velocities is not significant, axial velocity distribution is not trivial at all (Fig. 12) and the acceleration of the gas flow around the discharge channel is very obvious.

Discharge cross section grows with time and the shape of the cross section changes from the circular one (Fig. 12) to the bullet shape (Fig. 13), because of the interaction with low-temperature walls. Fig. 14 shows, the evolution of GA maximal temperature and axial position of the maximal temperature spot on time. At this higher current of 35 mA, maximal discharge temperature drops during the whole cycle after the initial channel formation stage.

Regime of 3 mA–10 m/s was simulated in laminar and turbulent conditions as well. Fig. 15 shows, the gas temperature distribution at the time step of 0.13 s for a laminar case. Three-angular shape of the discharge is even more pronounced than in the 3 mA–1 m/s case. Comparison of the maximal temperature between these two cases (1260K at 1 m/s versus 647K at 10 m/s) that differs only by the initial gas velocity clearly emphasizes the importance of convective

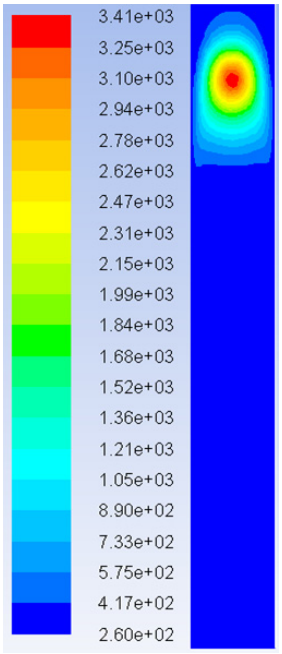

Fig. 13. Contours of gas temperature T_0(K) at time step of 0.11 s for 35 mA–1 m/s case.

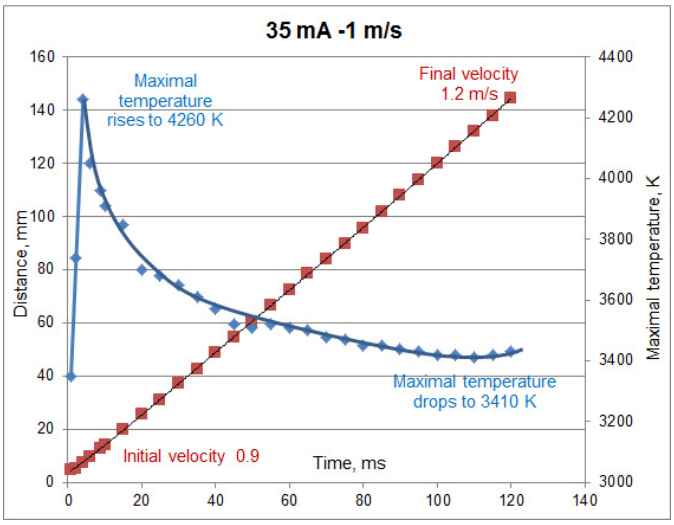

Fig. 14. Evolution of GA maximal temperature and axial position of the maximal temperature spot for 35 mA–1 m/s case.

discharge cooling. Non-trivial temperature distribution below the discharge is related to gas acceleration and deceleration in this area (compare with Fig. 12).

The velocity of 10 m/s should cause some turbulence in the 2 cm wide channel; therefore it was reasonable to study the turbulence effect. Initially, the flow was simulated without the discharge to find the input turbulence level that produces stable turbulence parameters along the channel. This corresponds to the fully developed flow in this flat channel. It was found that the initial turbulence intensity should be low, only 1%. Nevertheless, it is possible to see (Fig. 16) that in the main flow, the effective viscosity is more than ten times larger than the molecular one.

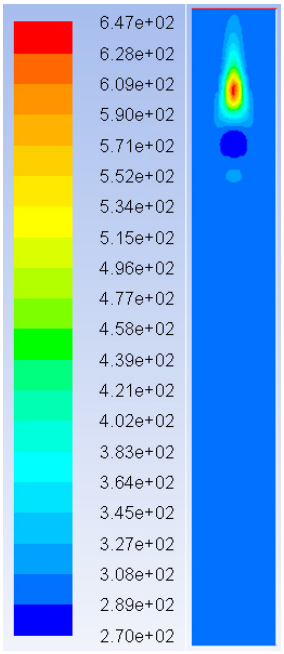

Fig. 15. Contours of gas temperature T_0 (K) at time step of 0.13 s for 3 mA–10 m/s laminar case.

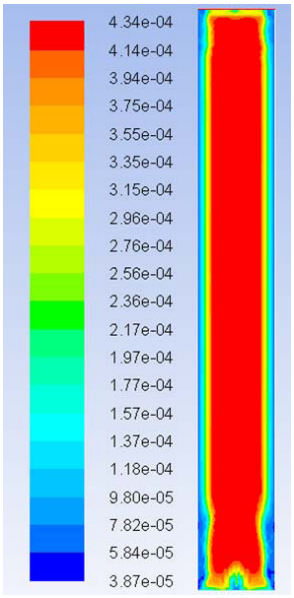

Fig. 16. Contours of effective viscosity (kg/m/s) in a flat channel without discharge with the initial turbulence level of 1%.

Simulation of the discharge with and without turbulence showed rather small though visible difference in the results (Fig. 17). The difference is small because even very low current of 3 mA significantly heats gas and suppresses turbulence because of the increase in gas viscosity. After that turbulence development takes significant time as it can be seen in Fig. 18.

In turbulent flow, discharge acceleration is faster because of higher viscosity and maximal temperature is lower because of higher heat conductivity (Fig. 17). Shape of the discharge cross section in the turbulent case is rather similar to that in thee laminar case (Fig. 15).

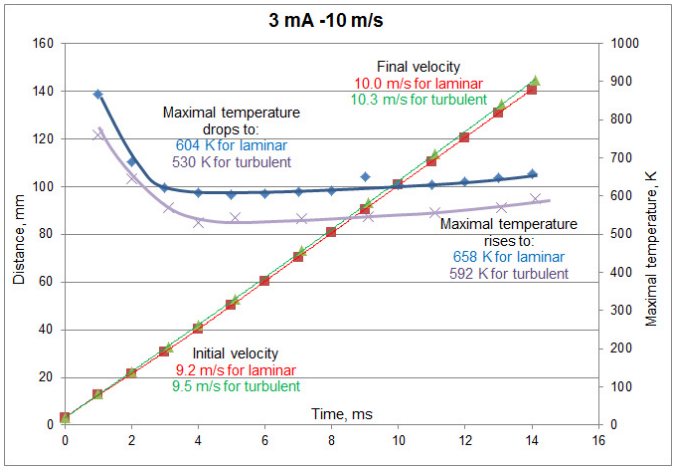

Fig. 17. Evolution of GA maximal temperature and axial position of the maximal temperature spot for 3 mA–10 m/s laminar and turbulent cases.

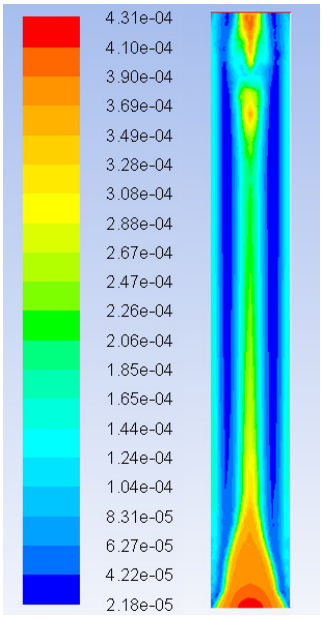

Fig. 18. Contours of effective viscosity (kg/m/s) at time step of 13 ms for 3 mA–10 m/s turbulent case.

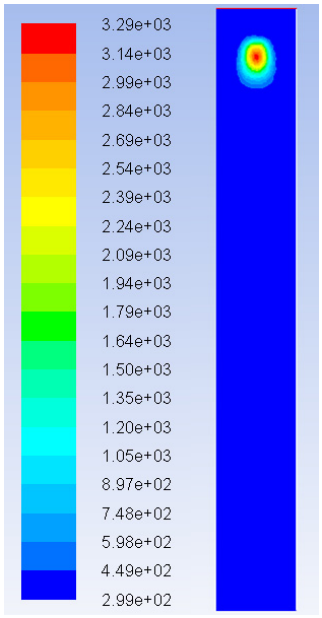

Fig. 19. Contours of gas temperature T_0(K) at time step of 13 ms for 35 mA–10 m/s case.

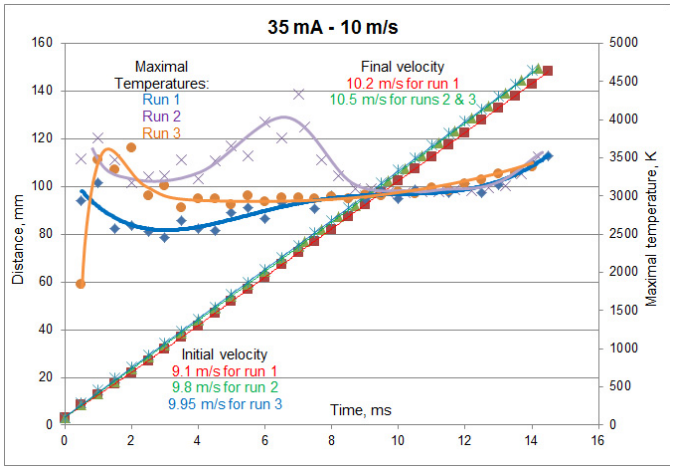

Fig. 20. Evolution of GA maximal temperature and axial position of the maximal temperature spot for three runs of the 35 mA–10 m/s case.

Considering rather small differences between the discharges in laminar and the turbulent 3 mA–10 m/s cases, and our goal of qualitative description of the discharge–flow interaction, the next cases with higher currents were simulated only in laminar regimes.

The case of 35 mA–10 m/s was run three times, because the results were slightly different. For this case, each run was rather long (8–20 hours) to ensure convergence on each time step. It is possible that during initial runs there were time steps without good convergence. In the last case, the time step was chosen to be small enough, 0.02 ms, to avoid any convergence problems. The biggest difference in the discharge appearance was visible in the very beginning of the development cycle that cannot represent physical reality because of the oversimplified approach to the discharge initiation stage (see the model description above). Nevertheless, the discharge simulation "remembers" this difference. Thus, the first run resulted in three-angle shape discharge cross section, similar to the case of 3 mA–10 m/s, while other runs resulted in oval shape of the discharge (Fig. 19). The discharge cross section is much smaller than that in the 35 mA–1 m/s case that indicates that the convective cooling in faster flow is much more efficient despite rather small gas-discharge slip velocity. Problems with simulation repeatability for this case are shown in Fig. 20. Nevertheless, at the ends of simulated cycles, discharge parameters came to almost the same values. For the second and third runs, electric field values E were also recorded. Fig. 21 shows that a spike in maximal gas temperature is associated with the significant drop of E.

The most interesting results were obtained for the case of 350 mA–10 m/s. This current value is typical for 1 kW power range GA. To have convergence at each time step,

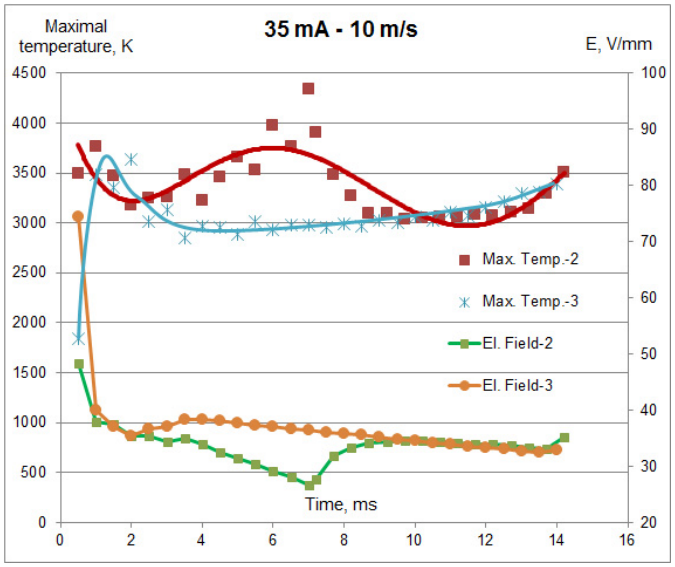

Fig. 21. Evolution of GA maximal temperature and electric field value E for the last two runs of the 35 mA–10 m/s case.

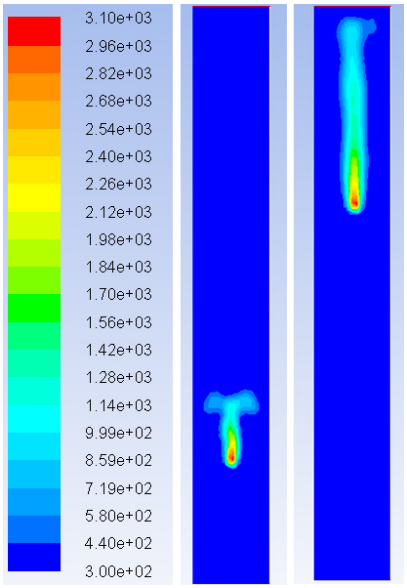

Fig. 22. Contours of gas temperature T_0 (K) at time steps of 4 and 13 ms for 350 mA–10 m/s case.

the step duration was reduced to the very low value of 5 ns. Total run time was more than two weeks. The grid size is small but the case was not modified for parallel computing, therefore the desktop computer did not run at full power. Nevertheless, this shows how time consuming transient case simulation can be.

Observe the discharge shape (Fig. 22). It is absolutely different from anything presented above. Appearance of "ears" can be related to the initially rather large area of patched high temperature region. However, elongation of the discharge region along the flow is probably a specific feature of the relatively high current discharge at relatively high speed gas flow.

Note, that it is probably impossible to reveal significant discharge elongation using photo or video recording, because rather small high temperature zone should be much

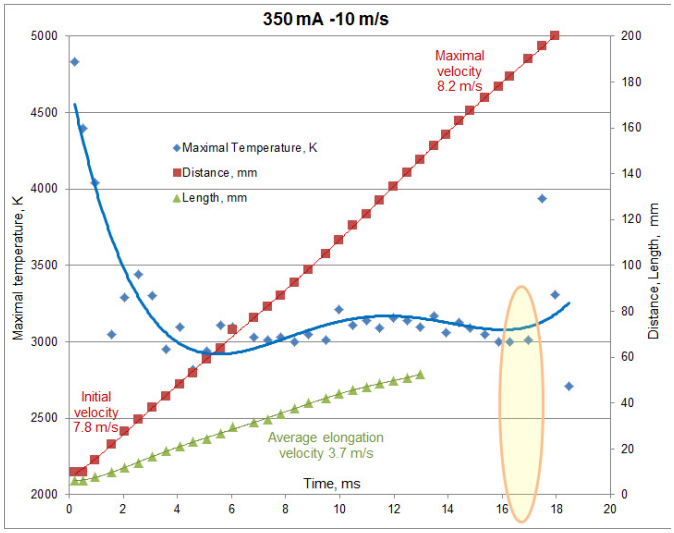

Fig. 23. Evolution of GA maximal temperature, axial position of the maximal temperature spot, and discharge elongation along the gas flow for the 350 mA–10 m/s case.

brighter than the rest of the electrically conductive channel. Multiple high resistance voltage probes inserted into the central portion of the flat GA discharge reactor walls can probably clarify this issue. We are unaware of any such experimental efforts. On the other hand, we also do not know of any publication that predicted such a significant discharge channel elongation in gas flow.

In this case, in contrast with all previously considered cases, the velocity of the maximal temperature spot did not reach the gas velocity (Fig. 23), thus the gas-discharge slip velocity is very significant. This is in agreement with significant slip velocities reported earlier and very recently [30], when the authors used a rather elaborated approach.

Analysis of the results of this run showed that in addition to the motion of the high temperature spot, it was significant and almost constant speed of the discharge cross-sectional elongation (Fig. 23). Note that our model does not include electromagnetic forces, which are assumed to be small. However, these forces cause "pinch effect" at high current discharges and can affect the discharge cross-sectional elongation. We hope that in the future numerical simulation modeling, especially for 3-D cases, other researchers will consider these forces. The PLASMANT Group in their published research [12]–[14] also did not include electromagnetic forces that can affect shape and size of the discharge cross section and discharge channel bending as well.

At the second half of the discharge lifecycle (350 mA–10 m/s case), the maximal temperature stabilized around 3000 K, similar to the case with 35 mA at 10 m/s. During this very long run, we periodically checked the progress and observed chaotic fluctuation of the electric field in a very wide range, and uncorrelated maximal temperature fluctuation but in a much narrower range. To understand what is going on, a short part of the case was rerun and the simulation results with electric field and gas temperature records were saved much more often than in the initial run (Fig. 24). Then, selections of the appropriate graphic scales

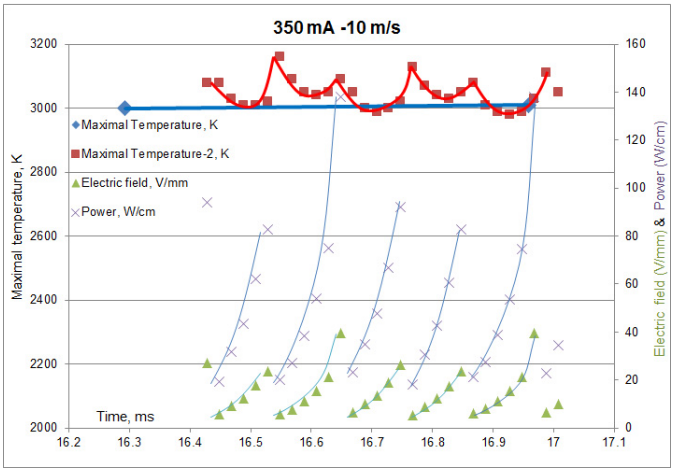

Fig. 24. Evolution of GA maximal temperature, electric field value E, and discharge power per unit of the discharge length for the 350 mA–10 m/s case. The case was rerun between 16.4 and 17 ms (highlighted area in Fig. 23).

revealed an interesting tendency. First of all, even in the selected simulation period when maximal temperature looks constant at relatively large time scale, there are wave-shaped oscillations of this value visible at smaller time scale. It is possible to see that fluctuation of the electric field amplitude and therefore power oscillations are really very big, minimal and maximal values can differ by a factor of 7. It looks like the maximums of the temperature waves correspond to the sudden drops in electric field value. This may be an artifact of the "broken" conductivity curves (Fig. 5). Nevertheless, it is clear that this kind of electric field oscillation can have the major effect on nonequilibrium plasma chemistry. For the experimental conditions, where the current over the whole length of the discharge is the same, but all other conditions, including the angle between the gas flow and the current directions vary in the different parts of the discharge, it means that at the same moment of time plasma conditions, e.g., electric field value, in different parts of the discharge will be very different. We are unaware of attempts to measure electric field distribution along a gliding discharge.

In the recent publication [30], the authors report on their experimental observation of the low current discharge from two different perpendicular directions. If to stop their movie available online at one-third of the movie length, when one camera looks along the upper portion of the discharge channel and therefore another camera looks straight to this discharge portion, it is possible to see that the brightness at the top of the discharge is much higher than at all other parts of the discharge. It is clear that this portion has higher temperature, larger cross section and, therefore, much lower electric field. Note that the authors found that gas-discharge slip velocity is in the range of 2–8 m/s with average of 4.5 m/s, while the gas velocity did not exceed 10 m/s. Looking at their experimental results, our simulation results, some GAT movies that we have, or pictures of the flat GA (Fig. 8), or magnetic GA [25], we got an impression that the role of "dragging" force from the electrode spots may be over-emphasized by some authors, e.g., [12], and the discharge elongation is caused mostly by nonuniform gas velocity distribution and presence of gas velocity components along the discharge channel. Thus, slip velocity can be also caused by other reasons as the last simulation case shows.

Note that discharge channel cross-sectional elongation in the direction of the slip velocity can provide additional stability to gliding discharges in the advanced systems, such as magnetically stabilized GA [25], [26] or GAT flow [27], [28].

IV. Conclusion

Our simulation shows that transverse 2-D GA modeling can give very useful information about the gas-discharge interaction. Thus, gas-discharge slip velocity exists at least at the beginning of a cycle even if there is no mechanism for discharge deceleration. Just original spark formation associated with the electrode surfaces results in the appearance of this "independent" slip. In the cases of reasonably high gas velocities and discharge currents, this initial slip does not disappear during the discharge lifetime and can result in significant discharge cross-sectional elongation along the gas flow. Electric field difference between different parts of the discharge channel and the field fluctuation at any particular part of the channel can be very large, and this can have the major effect on the nonequilibrium ionization and chemical processes.

References

[1] A. Czernichowski, "Gliding arc: Applications to engineering and environment control," *Pure Appl. Chem.*, vol. 66, no. 6, pp. 1301–1310, Jan. 1994.

[2] C. S. Kalra, A. F. Gutsol, and A. A. Fridman, "Gliding arc discharges as a source of intermediate plasma for methane partial oxidation," *IEEE Trans. Plasma Sci.*, vol. 33, no. 1, pp. 32–41, Feb. 2005.

[3] J. O. Pacheco-Sotelo *et al.*, "An environmental application in acid gas cracking with a high-frequency pulsed gliding arc," *IEEE Trans. Plasma Sci.*, vol. 42, no. 3, pp. 767–773, Mar. 2014.

[4] C. Du *et al.*, "Decontamination of bacteria by gas-liquid gliding arc discharge: Application to *Escherichia coli*," *IEEE Trans. Plasma Sci.*, vol. 42, no. 9, pp. 2221–2228, Sep. 2014.

[5] T.-L. Zhao *et al.*, "Dynamic evolution of 50-Hz rotating gliding arc discharge in a vortex air flow," *IEEE Trans. Plasma Sci.*, vol. 42, no. 10, pp. 2704–2705, Oct. 2014.

[6] L. Potočňáková, J. Šperka, P. Zikán, J. J. W. A. van Loon, J. Beckers, and V. Kudrle, "Gliding arc in noble gases under normal and hypergravity conditions," *IEEE Trans. Plasma Sci.*, vol. 42, no. 10, pp. 2724–2725, Oct. 2014.

[7] F. Mitsugi *et al.*, "Gas flow dependence on dynamic behavior of serpentine plasma in gliding arc discharge system," *IEEE Trans. Plasma Sci.*, vol. 42, no. 12, pp. 3681–3686, Dec. 2014.

[8] A. J. Wu, H. Zhang, X. D. Li, S. Y. Lu, C. M. Du, and J. H. Yan, "Determination of spectroscopic temperatures and electron density in rotating gliding arc discharge," *IEEE Trans. Plasma Sci.*, vol. 43, no. 3, pp. 836–845, Mar. 2015.

[9] A. F. Bublievsky *et al.*, "Similarity relations of power–voltage characteristics for tornado gliding arc in plasma-assisted combustion processes," *IEEE Trans. Plasma Sci.*, vol. 43, no. 5, pp. 1742–1746, May 2015.

[10] W. W. Wu, G. H. Ni, Q. F. Lin, Q. J. Guo, and Y. D. Meng, "Experimental investigation of premixed methane–air combustion assisted by alternating-current rotating gliding arc," *IEEE Trans. Plasma Sci.*, vol. 43, no. 12, pp. 3979–3985, Dec. 2015.

[11] A. El-Zein, M. Talaat, G. El-Aragi, and A. El-Amawy, "Electrical characteristics of nonthermal gliding arc discharge reactor in argon and nitrogen gases," *IEEE Trans. Plasma Sci.*, vol. 44, no. 7, pp. 1155–1159, Jul. 2016.

[12] S. Kolev and A. Bogaerts, "A 2D model for a gliding arc discharge," *Plasma Sour. Sci. Technol.*, vol. 24, no. 1, pp. 015025-1–015025-16, Feb. 2015.

[13] S. Kolev and A. Bogaerts, "Similarities and differences between gliding glow and gliding arc discharges," *Plasma Sour. Sci. Technol.*, vol. 24, no. 6, pp. 065023-1–065023-8, Dec. 2015.
[14] G. Trenchev, S. Kolev, and A. Bogaerts, "A 3D model of a reverse vortex flow gliding arc reactor," *Plasma Sour. Sci. Technol.*, vol. 25, no. 3, pp. 035014-1–035014-12, Jun. 2016.
[15] G. A. Saevarsdottir, H. L. Larsen, and J. A. Bakken, "Modelling of industrial AC-arcs," *High Temperature Mater. Process., Int. Quart. High-Technol. Plasma Process.*, vol. 3, no. 1, pp. 1–15, 1999.
[16] C. Rehmet, F. Fabry, V. Rohani, F. Cauneau, and L. Fulcheri, "Unsteady state analysis of free-burning arcs in a 3-Phase AC plasma torch: Comparison between parallel and coplanar electrode configurations," *Plasma Sour. Sci. Technol.*, vol. 23, no. 6, pp. 065011-1–065011-12, Dec. 2014.
[17] L. Fulcheri, F. Fabry, S. Takali, and V. Rohani, "Three-phase AC arc plasma systems: A review," *Plasma Chem. Plasma Process.*, vol. 35, no. 4, pp. 565–585, Jul. 2015.
[18] Y. D. Korolev, O. B. Frants, N. V. Landl, A. V. Bolotov, and V. O. Nekhoroshev, "Features of a near-cathode region in a gliding arc discharge in air flow," *Plasma Sour. Sci. Technol.*, vol. 23, no. 5, pp. 054016-1–054016-10, Oct. 2014.
[19] T. Farouk, B. Farouk, D. Staack, A. Gutsol, and A. Fridman, "Simulation of dc atmospheric pressure argon micro glow-discharge," *Plasma Sour. Sci. Technol.*, vol. 15, no. 4, pp. 676–688, Nov. 2006.
[20] F. Kannari, A. Suda, M. Obara, and T. Fujioka, "Theoretical simulation of electron-beam-excited xenon-chloride (XeCl) lasers," *IEEE J. Quantum Electron.*, vol. 19, no. 10, pp. 1587–1600, Oct. 1983.
[21] S. V. Dresvin, *Osnovy Teorii i Rascheta Vysokochastotnykh Plazmotronov*, (in Russian), Leningrad, Russia: Energoatomizdat, 1991, pp. 1–312.
[22] Y. P. Raizer, *Gas Discharge Physics*. Berlin, Germany: Springer-Verlag, 1991, pp. 1–449.
[23] A. Fridman, *Plasma Chemistry*. Cambridge, U.K.: Cambridge Univ. Press, 2008, pp. 1–978.
[24] I. V. Kuznetsova, N. Y. Kalashnikov, A. F. Gutsol, A. A. Fridman, and L. A. Kennedy, "Effect of 'overshooting' in the transitional regimes of the low-current gliding arc discharge," *J. Appl. Phys.*, vol. 92, no. 8, pp. 4231–4237, Oct. 2002.
[25] S. P. Gangoli, A. F. Gutsol, and A. A. Fridman, "A non-equilibrium plasma source: Magnetically stabilized gliding arc discharge: I. Design and diagnostics," *Plasma Sour. Sci. Technol.*, vol. 19, no. 6, pp. 065003-1–065003-7, Dec. 2010.
[26] S. P. Gangoli, A. F. Gutsol, and A. A. Fridman, "A non-equilibrium plasma source: Magnetically stabilized gliding arc discharge: II. Electrical characterization," *Plasma Sour. Sci. Technol.*, vol. 19, no. 6, pp. 065004-1–065004-6, Dec. 2010.
[27] C. S. Kalra, Y. I. Cho, A. Gutsol, A. Fridman, and T. S. Rufael, "Gliding arc in tornado using a reverse vortex flow," *Rev. Sci. Instrum.*, vol. 76, no. 2, pp. 025110-1–025110-7, Feb. 2005.
[28] A. F. Gutsol, "Gliding glow discharge in tornado," *IEEE Trans. Plasma Sci.*, vol. 39, no. 11, pp. 2086–2087, Nov. 2011.
[29] E. A. Haering, Jr., J. W. Smolka, J. E. Murray, and K. J. Plotkin. (2005). Flight demonstration of low overpressure N-wave sonic booms and evanescent waves. NASA. [Online]. Available: http://ntrs.nasa.gov/archive/nasa/casi.ntrs.nasa.gov/20050192479.pdf
[30] J. Zhu *et al.*, "Measurements of 3D slip velocities and plasma column lengths of a gliding arc discharge," *Appl. Phys. Lett.*, vol. 106, no. 4, pp. 044101-1–044101-4, Jan. 2015.

Alexander F. Gutsol received the B.S. and M.S. degrees in physics and engineering and the Ph.D. degree in physics and mathematics from the Moscow Institute of Physics and Technology, Moscow, Russia, in 1982 and 1985, respectively, and the D.Sc. degree in mechanical engineering for his achievements in plasma chemistry and technology from the Baykov Institute of Metallurgy and Material Science, Moscow, in 2000.

From 1985 to 2000, he was with the Kola Science Center, Institute of Chemistry and Technology of Rare Elements and Minerals, Russian Academy of Sciences, Apatity, Russia. He was a Visiting Researcher in Israel, in 1996, in Norway, in 1997, in The Netherlands, in 1998, and in Finland, from 1998 to 2000. Since 2000, he has been in USA, particularly with the University of Illinois at Chicago, Chicago, IL, USA, from 2000 to 2002, the A. J. Drexel Plasma Institute, Drexel University, Philadelphia, PA, USA, from 2002 to 2008, and has been with Chevron Energy Technology Company, Richmond, CA, USA, since 2008.

Shailesh P. Gangoli received the B.E. degree from Manipal University, Manipal, India, in 2002, and the M.S and Ph.D. degrees from Drexel University, Philadelphia, PA, USA, in 2007, all in mechanical engineering.

He subsequently joined Air Products, Allentown, PA, as a Senior Research Engineer (Ph.D. Career Development Program), where he was involved in the development of proprietary plasma and combustion technologies for effective utilization of industrial gases, such as O2, N2, and Ar, in a variety of industrial applications. He currently heads the Combustion Technology Development Group serving the Metals and Minerals industry customers of Air Products.